Inelastic muon-neutron scattering: Charged-hadron multiplicities and prong cross sections

K. Bunnell, M. Duong-van, R. Mozley, A. Odian, F. Villa, and L. C. Wang
Stanford Linear Accelerator Center, Stanford, California

C. del Papa,* D. Dorfan, S. M. Flatté, C. A. Heusch, B. Lieberman,† L. Moss, T. Schalk, and A. Seiden
University of California, Santa Cruz, California

(Received 19 December 1977)

Based on approximately 10000 inelastic muon scatters in a liquid deuterium target, we extract charged-hadron multiplicities and topological cross sections for events off the neutron in a range $0.3 \leq Q^2 \leq 4.5$ GeV^2, $2.0 \leq W \leq 4.6$ GeV. We find no significant changes in the multiplicity or topological fractional cross sections over the Q^2 range of our experiment. Empirically the average multiplicity off a neutron target is equal to that off a proton target over the Q^2 and W range of our experiment.

I. INTRODUCTION

Following an experiment which investigated muon-proton scattering,[1] we have performed, using the same apparatus, a second experiment with deuterium as a target. From the data obtained in both experiments, we have been able to extract fractional-prong cross sections and average multiplicities in the process $\mu n \to \mu +$ hadrons. Other results from these experiments will be published separately.

II. EXPERIMENTAL METHOD

The apparatus used in this experiment is the one described in Ref. 1. We mention only features that have a particular bearing on the data presented here.

A 14-GeV, low-halo, small-phase-space, positive-muon beam[2] was directed into a 40-cm-long liquid hydrogen or deuterium target placed inside a 2-m streamer chamber.[3] The chamber was located in a 16-kG magnetic field. The trigger system for the streamer chamber consisted of four hodoscopes imbedded in a 1.5-m lead wall, separating the final-state muon from hadrons.

Counters at the exit end and on the perimeter of the streamer chamber provide timing information used to reject δ rays, halo muons, and other spurious tracks. In order to reduce δ-ray tracks in the pictures, the noninteracting beam travels inside a 5-cm-diameter lexan tube, filled with helium gas; in addition, the target is enclosed in a mylar box containing teflon absorbers. This produces a neutral region aroung the target, where tracks with steeply dipping angles are lost.

For an accurate subtraction of proton events from a deuterium experiment, a precise measurement of the beam flux is necessary. An integrating Cherenkov monitor[4] was used to give this information to a precision of 3% over the course of this experiment.

III. ANALYSIS

Most of the data-reduction process in this experiment follows closely the procedure for muon-proton scattering described in Ref. 1. Some significant effects should be mentioned that arise due to the deuterium target.[5] The scanning rules define a picture as an event candidate if and only if it contains at least two positive tracks, one of which is consistent with being a triggering muon. All muon-proton events satisfy these criteria, but events of the type $\mu n \to \mu n +$ neutrals (zero-prong events) are systematically rejected. The cross section for this event type can be calculated, as discussed below, and in any case is a small fraction of the total.

We have applied no corrections to the data for the effect of Fermi motion, since its effect is small. An estimate of the size of this effect was obtained as follows: For each event in the data sample, we assign a value for the spectator momentum, with a probability given by the Hulthén nucleon wave function,[6] and recalculate the kinematics of the event. This gives us smeared distributions which can be compared with those resulting if we assume zero spectator momentum. Changes due to smearing, for the quantities presented in this paper, are less that 1 standard deviation everywhere. Furthermore, no radiative corrections were applied to the data. A detailed study involving a *proton* target showed that they affect the proton results by, typically, less than 10% (cf. Tables I and II, Ref. 1); for the *neutron* case, much of the effect would come from the radiative tail of elastic μn scatters. These, however, are not observed in our analysis anyway, since they are zero-prong events.

Because of the obstructions around the target and beam line in the chamber, we lose certain tracks. A Monte Carlo program assigns to each tracks, including that of the triggering muon, a

weight according to known geometry and efficiency effects. These weights were then used to correct for event losses for certain multiplicities, as discussed below.

IV. RESULTS

A. Elastic muon-proton scattering

In order to compare the hydrogen and deuterium experiments, we use normalization constants α_p, α_d, which define the ratio between the total number of events expected in each experiment for a given effective total cross section. Using a determination of the flux by our downstream monitor, we can extract α_p from the data of Ref. 1, α_d from the present experiment:

$\alpha_p = 54.4$ events/nb,

$\alpha_d = 64.8$ events/nb.

The study of the elastic channel $\mu p \to \mu p$ in both experiments gives us an independent way of measuring these constants, aside from providing a general check of our data. Elastic μp events are fully constrained kinematically (four-constraint fits), and are therefore easily picked up by the kinematics-reconstruction program, SQUAW. For the case of deuterium, the analogous fit is $\mu p(n_s) \to \mu p(n_s)$ where n_s is a neutron spectator. Dividing the number of such elastic events for deuterium by the number seen in the hydrogen experiment gives us α_d/α_p, which is the constant needed for the proton subtraction from deuterium.

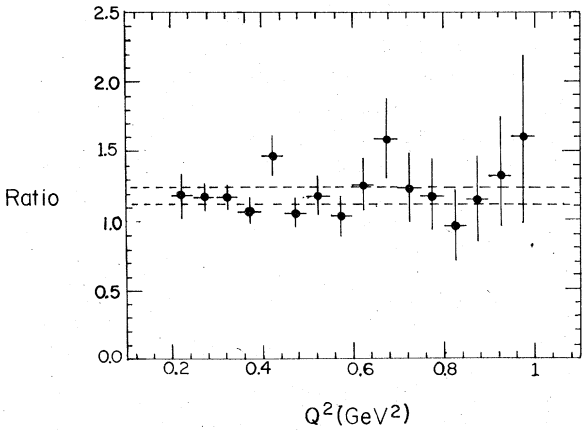

FIG. 1. Ratio of the number of reconstructed elastic muon-proton scatters for the deuterium target experiment as compared to the hydrogen target experiment, in bins of Q^2. The expected value, based on our beam-flux monitor and target density measurements, is 1.19 ± 0.05. The $+1\sigma$ and -1σ expected values are shown as dashed lines.

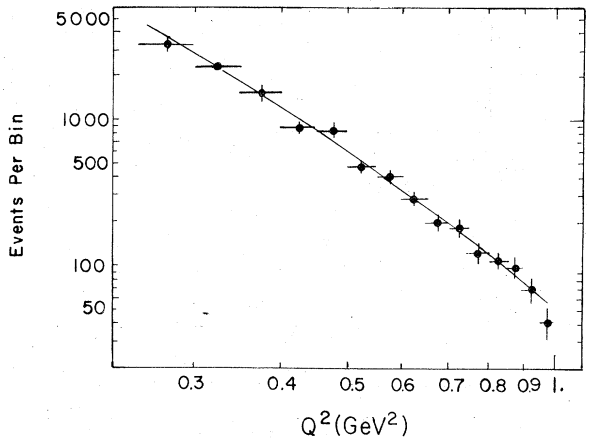

FIG. 2. A comparison of the expected (curve) and reconstructed number of elastic muon-proton scattering events for the hydrogen experiment. The expected value for a bin in Q^2 of width ΔQ^2, is $\alpha_p(d\sigma/dQ^2)\Delta Q^2$. where the elastic form factors used in calculating $d\sigma/dQ^2$ are given by the dipole formula $(1/1+Q^2/0.71)^2$. The reconstructed events have been weighted by the geometrical acceptance. No radiative corrections have been made.

The results, shown in Fig. 1, are in excellent agreement with the determination from the flux and target density monitors. The error on our measurement of α_d/α_p is 5% (with a 3% error for α_d, 4% for α_p), similar to the estimated systematic error in determining the number of elastic events in deuterium. Figure 2 shows the hydrogen data separately, checking the absolute value of α_p.

B. Zero-prong events

A zero-prong event is an event of the type $\mu n \to \mu n +$ neutrals. These events are *not* picked up by the scanners. Their fractional occurrence can be calculated by comparing the total number of neutron events we see with the number of events expected according to the known total cross section. Denote with σ_i^n, σ_0^n the cross sections in collisions off the neutron with i (one or several) charged hadrons in the final state, or with no charged hadrons at all, respectively. In addition, denote with σ^p, σ^n the total cross section for collisions with proton or neutron targets. We then have for a given Q^2 and W,

$$R = \frac{\sigma_i^n}{\sigma^p} = \left[\frac{\sigma^n - \sigma_0^n}{\sigma^n}\right]\frac{\sigma^n}{\sigma^p} = (1 - f_0)\left(1 - x + \frac{x^3}{4}\right),$$

where $x = Q^2/(W^2 + Q^2)$ is the Bloom-Gilman scaling variable, $f_0 = \sigma_0^n/\sigma^n$ is the fractional cross-section for zero-prong events, and the polynomial in x is our own parametrization of the measured

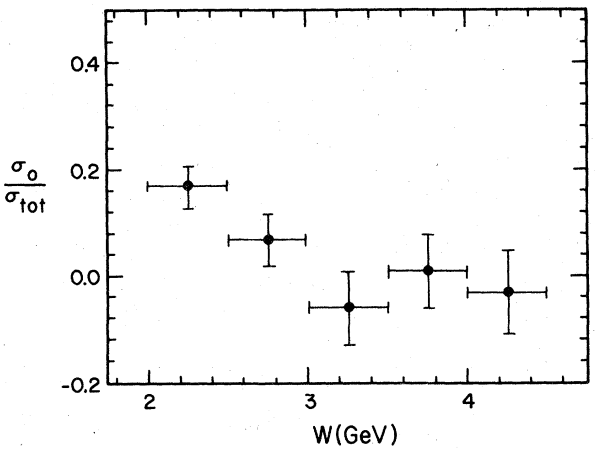

FIG. 3. The calculated zero-prong fraction of the total neutron cross section for five bins in W.

ratio for neutron and proton cross sections.[7] In calculating R from the data, the proton cross sections are obtained from the observed number of events in our hydrogen target experiment,[1] using α_p for normalization. The neutron cross sections are similarly obtained from deuterium after subtraction of the proton component of the cross section.

Solving for f_0, we find

$$f_0 = 1 - R\left(1 - x + \frac{x^3}{4}\right)^{-1}.$$

In Fig. 3, we show the result of our evaluation of f_0. It is binned in five W intervals, summed over a Q^2 range given by $0.5 \leq Q^2 \leq 4.5$ GeV^2. Our results are in good agreement with those of Ref. 8.

As a rule, we will present our data without corrections for the missing zero-prong events, with primes attached to uncorrected quantities. Where comparisons with particular data make an inclusion of the correction necessary, we use unprimed symbols. For the correction, we use for the zero-prong fraction

$$f_0 = \begin{cases} 0.2(3 - W), & 2.0 \leq W \leq 3.0 \text{ GeV}, \\ 0, & 3.0 \text{ GeV} < W, \end{cases}$$

with an uncertainty, δf_0, of 0.05 throughout.

C. Average charged-hadron multiplicities

In the ideal case (no visible spectator, all charged secondaries from the $\gamma^* n$ collision yield visible tracks), for a deuteron target, events off the proton can be separated from those off the neutron by using charge conservation. In practice, for our experiment, corrections must be made for cases where tracks are lost and for cases where the spectator proton is visible in the streamer chamber. We can, however, assume to good accuracy (as determined to 2% in the hydrogen experiment[1]) that, at most, one track is lost in any given event. For our configuration, $(5 \pm 3)\%$ contain visible spectator protons. An appropriate correction was introduced for each topology separately. Based on the above, our analysis assigns, for each deuterium event, neutron topologies as follows:

(1) Define: m = number of positive minus number of negative hadron tracks.

(2) For $m \geq 2$, we assume the event occurred on the proton with a negative hadron lost, so the event is eliminated from the neutron sample.

(3) For $m = 1$ or -1, we assume the event is a neutron event with a negative or positive hadron, respectively, lost. This track is therefore restored in the count of how many hadronic prongs were produced.

(4) For $m = 0$, all tracks are assumed to be seen, and the event is taken to be a neutron event.

The above procedure is then repeated for the hydrogen data, using α_d / α_p as a weight, allowing us to subtract out all those events which, although defined as neutron event candidates by the above procedure, were actually due to μp collisions. A special correction is needed for two-prong neutron events where a missing positive hadron causes the event to be rejected by our scanning criteria. The latter requires a 15% correction for the two-prong cross section, as calculated by the Monte Carlo track-weighting program. This is the only case where the Monte Carlo results are needed.

Using the above procedure, we calculate topological and total cross sections for neutron targets for various bins in Q^2 and W, and compare with our previously published data for proton targets.[1] Defining $f_n = \sigma_n / \sigma_{tot}$, where n = number of charged hadrons in the final state, we calculate average multiplicities as follows:

$$\langle n \rangle_p = \sum_{n=1,3\ldots} n f_n,$$

$$\langle n \rangle'_n = \sum_{n=2,4\ldots} n f'_n \quad \text{(no zero prongs)},$$

$$\langle n \rangle_n = \langle n \rangle'_n (1 - f_0) \quad \text{(corrected for zero prongs)}.$$

Note that the subscripts for the *left-hand side* refer to proton and neutron, respectively. We show in Fig. 4 the Q^2 dependence of $\langle n \rangle_p$ and $\langle n \rangle'_n$ for three bins in W. There is no statistically significant Q^2 dependence in either $\langle n \rangle_p$ or $\langle n \rangle'_n$ for the full Q^2 range of our experiment. To display the W dependence, we sum over $0.5 \leq Q^2 \leq 4.5$ and display the results in Fig. 5. For a more meaningful

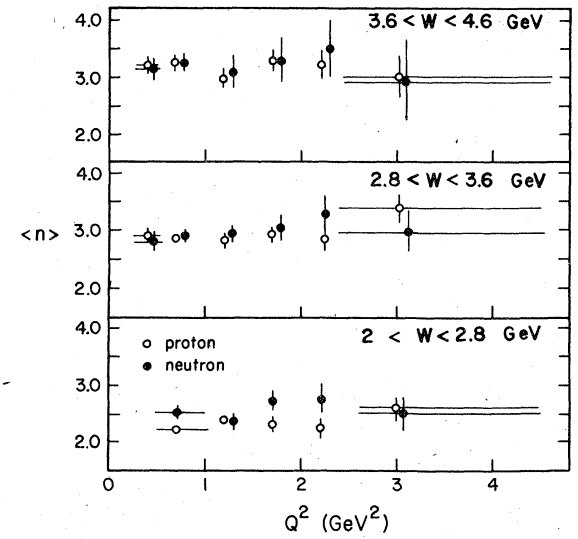

FIG. 4. Average charged-hadron multiplicities versus Q^2, in three W bands, for μ-p and μ-n events. Zero-prong events have not been corrected for, since the main point of this figure is the Q^2 dependence.

comparison at low W, the zero-prong correction has been included for the neutron case in this figure. It is seen that:

(1) $\langle n\rangle_n \simeq \langle n\rangle_p$ over nearly the whole energy range, for $2.0 \leq W \leq 4.6$ GeV.

(2) the energy trend of $\langle n\rangle p$ and $\langle n\rangle_n$ is compatible with a ln$s$ behavior, a result familiar from purely hadronic reactions.

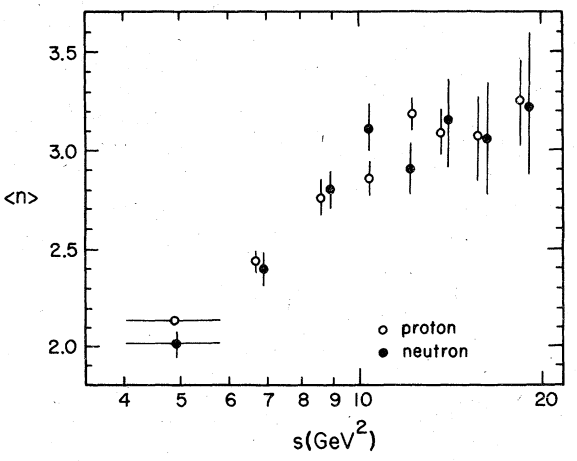

FIG. 5. Average charged-hadron multiplicities for proton and neutron targets versus ln s, for all Q^2 between 0.5 and 4.5 GeV^2. Zero-prong events have been included in the calculation for the neutron case, since this figure gives important comparisons between proton and neutron targets.

(3) in Ref. 1, it was shown that the average multiplicity from a proton target was closely equal to the values seen in various hadron-induced reactions. The equality of $\langle n\rangle_n$ and $\langle n\rangle_p$ therefore implies that the neutron target average multiplicity also agrees with these purely hadronic values.

It is perhaps surprising that the charge differences in the initial state (p versus n) do not result in different average multiplicities for the final state. We return to a quantitative discussion of this point in Sec. IV E.

D. Topological cross sections

We now discuss the charged prong, or topological, cross sections, which served as input to the above determination of $\langle n\rangle_{p,n}$. In Figs. 6–9, we display the Q^2 and W dependences of the f_n defined above, the fractional-prong cross sections, for various binnings. Note that n = odd refers to proton data, n = even $\neq 0$ to neutron data. Zero-prong data were not incorporated in the determinations shown in the first three figures; Figs. 6, 7, and 8 therefore do not normalize to the full total cross sections. The last figure, showing the W dependence, has been corrected for zero-prong events.

We observe the following points:

(1) There is no discernible variation with Q^2 in our data for either proton or neutron events.

(2) The W trend of the proton data, f_n (n = odd), can be characterized as follows:

(a) f_1 decreases considerably between $W = 2$ and 3 GeV, and then flattens out.

(b) f_3 remains roughly constant over the full W

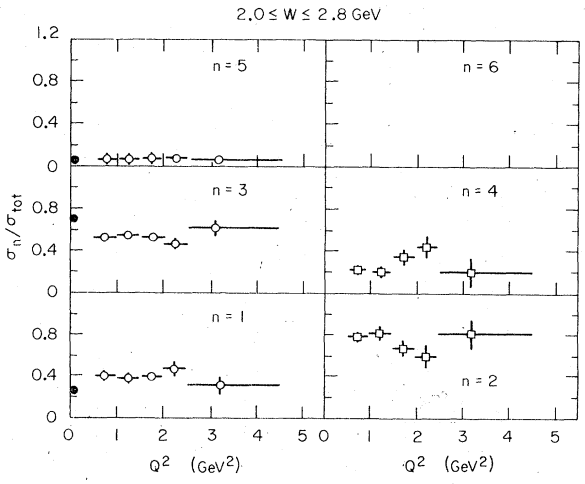

FIG. 6. Fractional topological cross sections versus Q^2 for proton and neutron targets for $2.0 \leq W \leq 2.8$ GeV. Zero-prong events have not been corrected for. Filled points are the analogous quantities measured in photoproduction on a hydrogen target.

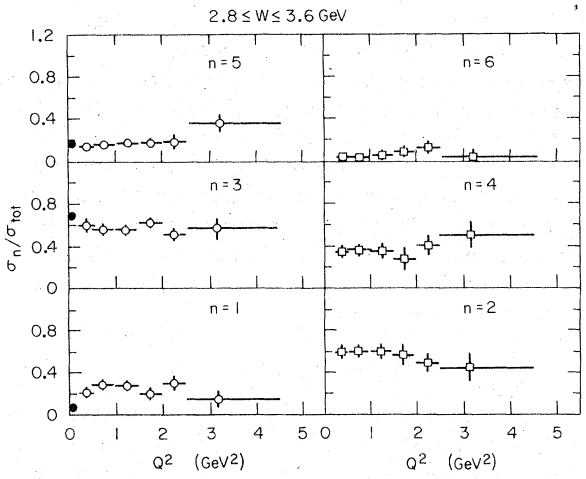

FIG. 7. Fractional topological cross sections versus Q^2 for proton and neutron targets for $2.8 \leq W \leq 3.6$ GeV. Zero-prong events have not been corrected for. Filled points are the analogous quantities measured in photoproduction on a hydrogen target.

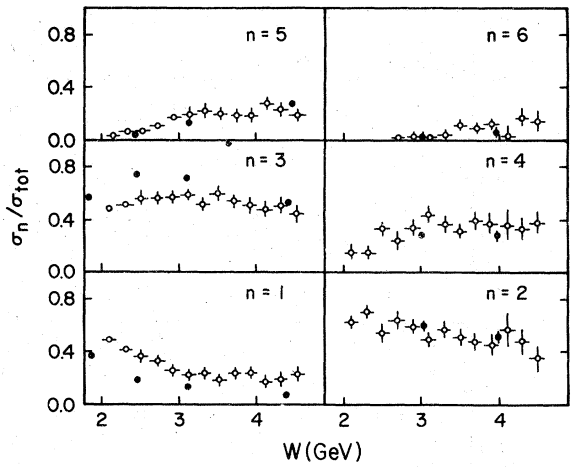

FIG. 9. W dependence of the fractional topological cross sections for all Q^2 between 0.5 and 4.5 GeV^2. Neutron and proton values are shown separately with analogous photoproduction results shown as solid points. Zero-prong events have been included for the neutron case.

range.

(c) f_5 opens up with phase space available and then also flattens.

(d) f_n for $n \geq 7$, not shown in the figure, is insignificant over our W range. Its phase space is just starting to open up at our highest W values.

(3) The fractional neutron cross sections, f_n (n = even), show the following pattern:

(a) f_0 decreases rapidly to zero between $W = 2$ and 3 GeV (cf. Fig. 3).

(b) f_2 decreases slowly over the full W range.

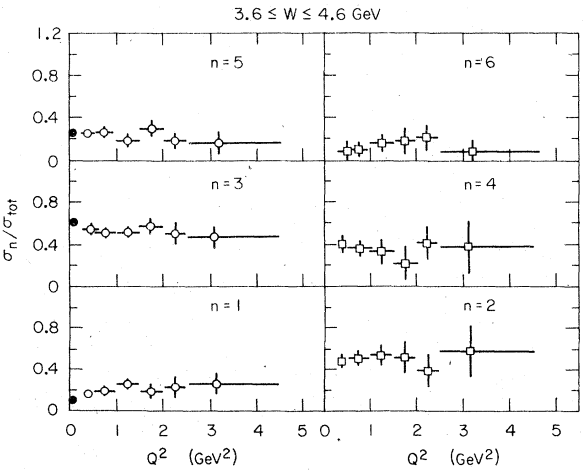

FIG. 8. Fractional topological cross sections versus Q^2 for proton and neutron targets for $3.6 \leq W \leq 4.6$ GeV. Zero-prong events have not been corrected for. Filled points are the analogous quantities measured in photoproduction on a hydrogen target.

(c) f_4 increases with the available phase space.

(d) f_6 opens up with phase space.

(4) There are considerable differences in f_1 and f_3 when compared with photoproduction data.[9] These have been described in detail in Ref. 1.

As an overall result, we find again, as in the proton case before, a remarkable constancy of fractional-prong cross sections with photon "mass-squared" Q^2.

E. Discussion of results on $\langle n \rangle$ and f_n

The data in Sec. IV C have shown that the charged-hadron multiplicities for both neutron and proton targets are closely similar. At first sight this result may appear surprising, since the proton initial state has one extra unit of charge. In this section we show qualitatively how such a result can plausibly arise.

Consider the various possible ways in which the initial-state baryon (proton or neutron) may emerge in the final state. Ignoring strange baryon and baryon-antibaryon production, which are small at our energies, we define

$$\left.\begin{aligned}\gamma^* p &\to p + \cdots \\ \gamma^* n &\to n + \cdots\end{aligned}\right\} \text{as direct channels,}$$

$$\left.\begin{aligned}\gamma^* p &\to n\pi^+ + \cdots \\ \gamma^* n &\to p\pi^- + \cdots\end{aligned}\right\} \text{as exchange channels.}$$

The separation into direct and exchange channels is a useful distinction since these receive contributions from different particle exchanges in the simplest cases. For example, for the lowest multiplicities in μn and μp reactions we have

$$\left.\begin{matrix}\gamma^* p \to p\pi^0 \\ \gamma^* n \to n\pi^0\end{matrix}\right\}\text{leading exchange: } \omega^0 \text{ (natural } J^P\text{)},$$

$$\left.\begin{matrix}\gamma^* p \to n\pi^+ \\ \gamma^* n \to p\pi^-\end{matrix}\right\}\text{leading exchange: } \pi \text{ (unnatural } J^P\text{)}.$$

Therefore the cross section for these will be quite different.

At this point we make two simplifying assumptions, not because they are particularly justifiable, but only to provide an illustration of a possible multiplicity relation between neutron and proton targets. The assumptions are negligible strange-particle production, and negligible effects of the isospin interference terms that arise from the mixed isospin character of the photon. If these assumptions were valid, then the two direct-channel processes would have equal cross sections, reaction by reaction, as would the two exchange-channel processes. If the direct channels dominated, it would follow that $\langle n\rangle_p = \langle n\rangle_n + 1$. On the other hand, if the exchange channels dominated, $\langle n\rangle_p = \langle n\rangle_n - 1$.

Experimentally, photoproduction results yield $\langle n\rangle_p \simeq \langle n\rangle_n + \frac{1}{2}$, while our experiment at $Q^2 \neq 0$ gives $\langle n\rangle_p \simeq \langle n\rangle_n$. One would conclude then that in photoproduction the direct channels dominate,[10] while for $Q^2 \neq 0$ our observations imply that direct and exchange processes are approximately equal.

This illustrative example has shown how an equality of the charged multiplicity from proton and neutron targets could arise from the effects of direct and exchange reactions. However, strange-particle production, and isoscalar-isovector interference terms could both have effects on the multiplicity relation. To disentangle the relative importance of these processes would require considerably more detailed information about many exclusive reactions.

ACKNOWLEDGMENT

This work was supported in part by the U. S. Department of Energy.

---

*Now at CERN, Geneva, Switzerland.
†Now at ETEC Corporation, Hayward, California.

[1]C. del Papa *et al.*, Phys. Rev. D 13, 2934 (1976).
[2]S. M. Flatté, C. A. Heusch, and A. Seiden, Nucl. Instrum. Methods 119, 333 (1974).
[3]C. A. Heusch, B. Lieberman, and A. Seiden, Nucl. Instrum. Methods 124, 165 (1975).
[4]B. Lieberman, University of California at Santa Cruz Report No. 7i-003 (unpublished).
[5]Further details of experiment and data analysis can be found in C. del Papa, Ph.D thesis, University of California at Santa Cruz, 1976 (unpublished).
[6]L. Hulthén and M. Suguwara, Handb. Phys. 39, 1 (1957).
[7]S. Stein *et al.*, Phys. Rev. D 12, 1884 (1975).
[8]B. Gibbard *et al.*, Phys. Rev. D 11, 2367 (1975).
[9]J. Ballam *et al.*, Phys. Rev. D 5, 545 (1972); H. H. Bingham *et al.*, *ibid.* 8, 1277 (1973).
[10]G. Alexander *etal.*, Nucl. Phys. B 68, 1 (1974); Y. Eisenberg *et al.*, *ibid.* 104, 61 (1976).